AIAA-95-1690-CP

FULLY NON-LINEAR CFD TECHNIQUES FOR SHIP PERFORMANCE ANALYSIS AND DESIGN

J. Farmer * *L. Martinelli* § *G. Cowles* §§ and *A. Jameson* ‡
Department of Mechanical and Aerospace Engineering
Princeton University
Princeton, New Jersey 08544

Abstract

Non-oscillatory discretization methods based on the Local Extremum Diminishing principle, which were originally devised for compressible flow, are applied to the free-surface evolution equation. More specifically, both symmetric and upstream limited schemes are utilized in the calculation of the flow about the Series 60 hull, a naval frigate hull with sonar dome and transom stern, and a fully configured IACC yacht hull at an angle-of-attack. The new free surface discretization techniques improve the overall numerical approach which has become sufficiently accurate, robust, and efficient to be used routinely in a design environment.

Introduction

The prediction of the total drag experienced by an advancing ship is a complicated problem which requires a thorough understanding of the hydrodynamic forces acting on the ship hull, the physical processes from which these forces arise and their mutual interaction. For instance, it is well established that an advancing ship generates a complex flow field which consists of both the wave structure and the viscous boundary layer and wake. These two features of the flow field result in the well known drag components referred to as the wave resistance and the viscous resistance, respectively. The wave resistance arises from the continuous transfer of energy, from the ship's propulsor mechanism to the fluid, required to maintain the wave structure that extends well aft of the ship. The viscous resistance manifests itself through the stresses which act tangentially on the wetted surface of the ship hull, through the absence of "perfect fluid streamlines" due to boundary layer growth and separation and through the presence of vortices. It is also well established that the boundary layer and wake can influence the resulting wave structure through displacement thickness effects and the wave structure can influence the boundary layer through wave elevation and wave-induced pressure gradient effects [1, 2]. It is this mutual interaction that renders the prediction of the total drag of an advancing ship a challenging task, whether by experimental, analytical or computational methods.

The advent of powerful computers - exhibiting both fast processing speed and large storage capabilities - has now made possible computational solutions of the full set of mathematical equations which describe the coupled wave structure and viscous boundary layer interaction. Notable previous computational approaches in this area include: the finite difference, velocity-pressure coupling approach of Hino [3]; the finite volume, velocity-pressure coupling approach of Miyata *et. al.* [4]; and the interactive approach of Tahara *et. al.* [5] which combines the finite analytic approach of Chen *et. al.* [6] and the "SPLASH" panel method of Rosen *et. al.* [7]. These methods all represent major advances in the computational solution of the coupled wave structure and viscous boundary layer interaction problem as it applies to ship hulls in general. However, they are all computationally intensive, requiring significant amounts of CPU time, and more importantly, they all rely on a linearization of the free surface boundary conditions.

The motivation behind the present work follows directly from the shortcomings of the CFD techniques currently available for ship analysis and design. A method which is robust and accurate for realistic hull shapes will greatly enhance hull design capabilities - from the naval architect designing frigates and destroyers, to the sailing yacht designer optimizing the performance of an America's Cup hull. This task demands that techniques for incorporating the fully nonlinear free surface boundary condition be included in the CFD methodology. Such a capability facilitates maintaining the exact hull geometry as the water moves up and down the curved sides of the ship or yacht hull. It also facilitates accurate assessment of the wavemaking and viscous drag components since both of these require evaluation of the exact wetted surface area of the hull. In addition, application of the fully nonlinear free surface boundary condition is a step toward more accurately modeling the features of the waves themselves, near and away from the hull. The ability to model the fully nonlinear ship wave problem, in a robust and accurate fashion, is in and of itself still not sufficient for effective design practice. The numerical techniques used in the process must also be efficient such that the turn-around time between simulations is

* Research Associate
§Assistant Professor, Member AIAA
§§Graduate Student
‡Professor, AIAA Fellow

sufficiently rapid to allow incorporation of the numerical model into the actual design process.

This paper presents recent advances in our work to accomplish these goals. The basic flow solver methodology follows directly from that outlined in our previous publications [8, 9]. This approach has proven to be accurate. The use of a novel moving grid technique permits application of the fully nonlinear free surface boundary condition, which in turn allows the simulation of the interaction between wavemaking and the viscous boundary layer. The approach has also proven to be efficient through the use of convergence acceleration techniques similar to those used to model compressible flows [10]. The use of a new free surface discretization technique substantially improves the robustness of the method, and results in the ability to model the flow about realistic hulls - including full configuration sailing yachts and hulls with transom sterns. Furthermore, the new free surface routine reduces the computer time that previously was required by approximately 50 percent.

Mathematical Model

Figure 1 shows the reference frame and ship location used in this work. A right-handed coordinate system $Oxyz$, with the origin fixed at the intersection of the bow and the mean free surface is established. The z direction is positive upwards, y is positive towards the starboard side and x is positive in the aft direction. The free stream velocity vector is parallel to the x axis and points in the same direction. The ship hull pierces the uniform flow and is held fixed in place, ie. the ship is not allowed to sink (translate in z direction) or trim (rotate in $x-z$ plane).

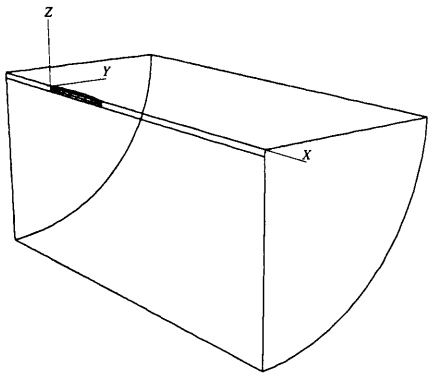

Figure 1: Reference Frame and Ship Location

Bulk Flow

For a viscous incompressible fluid moving under the influence of gravity, the differential form of the continuity equation and the Reynolds Averaged Navier-Stokes equations (RANS) may be put in the form [3],

$$u_x + v_y + w_z = 0 \tag{1}$$

$$\begin{aligned} u_t + uu_x + vu_y + wu_z &= -\psi_x + \left(Re^{-1} + \nu_t\right)\nabla^2 u \\ v_t + uv_x + vv_y + wv_z &= -\psi_y + \left(Re^{-1} + \nu_t\right)\nabla^2 v \\ w_t + uw_x + vw_y + ww_z &= -\psi_z + \left(Re^{-1} + \nu_t\right)\nabla^2 w. \end{aligned} \tag{2}$$

Here, $u = u(x,y,z,t)$, $v = v(x,y,z,t)$ and $w = w(x,y,z,t)$ are the mean total velocity components in the x, y and z directions. All lengths and velocities are nondimensionalized by the ship length L and the free stream velocity U, respectively. The pressure ψ is the static pressure p minus the hydrostatic component $-zFr^{-2}$ and may be expressed as $\psi = p + zFr^{-2}$, where $Fr = \frac{U}{\sqrt{gL}}$ is the Froude number. The pressure variable ψ is nondimensionalized by ρU^2. The Reynolds number Re is defined by $Re = \frac{UL}{\nu}$ where ν is the kinematic viscosity of water and is constant. The dimensionless turbulent eddy viscosity ν_t is computed locally throughout the flow domain using the Baldwin-Lomax turbulence model [9, 11].

For the inviscid case the viscosity coefficients are set to zero and the RANS equations 2 reduce to to the incompressible Euler equations, expressed here in differential vector form as

$$\mathbf{q}_t + \mathbf{q}\cdot\nabla\mathbf{q} = -\nabla\psi$$

where $\mathbf{q}$ is the velocity vector.

Boundary Conditions

Free Surface

When the effects of surface tension and viscosity are neglected, the boundary condition on the free surface consists of two equations. The first, the dynamic condition, states that the pressure acting on the free surface is constant. The second, the kinematic condition, states that the free surface is a material surface: once a fluid particle is on the free surface, it forever remains on the surface. The dynamic and kinematic boundary conditions may be expressed as

$$p = constant$$

$$\frac{d\beta}{dt} = w = \beta_t + u\beta_x + v\beta_y \tag{3}$$

where $z = \beta(x,y,t)$ is the free surface location.

Hull and Farfield

The remaining boundaries consist of the ship hull, the boundaries which comprise the symmetry portions of the meridian plane and the far field of the computational domain. On the ship hull, the condition is that of no-slip for the viscous formulation and flow tangency for the inviscid formulation. These conditions are stated mathematically as

$$u = v = w = 0$$

and

$$\mathbf{q}\cdot\mathbf{n} = un_x + vn_y + wn_z = 0.$$

On the symmetry plane (that portion of the (x,z) plane excluding the ship hull) derivatives in the y direction as well as the v component of velocity are set to zero. The upstream plane has $u = U_o$, $v = 0$, $w = 0$ and $\psi = 0$ ($p = -zFr^{-2}$). Similar conditions hold on the outer boundary plane which is assumed far enough away from the hull such that no disturbances are felt. A radiation condition should be imposed on the outflow domain to allow the wave disturbance to pass out of the computational domain. Although fairly sophisticated formulations may be devised to represent the radiation condition, simple extrapolations proved to be sufficient in this work.

Numerical Solution

The formulation of the numerical solution procedure is based on a finite volume method (FVM) for the bulk flow variables (u, v, w and ψ), coupled to a finite difference method for the free surface evolution variables (β and ψ).

Bulk Flow Solution

The FVM solution for the bulk flow follows the same procedures that are well documented in references [8, 9]. The governing set of differential flow equations are expressed in the standard form for artificial compressibility as [12]

$$\mathbf{w}_{t^*} + (\mathbf{f} - \mathbf{f_v})_x + (\mathbf{g} - \mathbf{g_v})_y + (\mathbf{h} - \mathbf{h_v})_z = 0 \qquad (4)$$

where $\mathbf{w}$ is the vector of dependent variables, and $\mathbf{f}, \mathbf{g}, \mathbf{h}$ and $\mathbf{f_v}, \mathbf{g_v}, \mathbf{h_v}$ are the vectors which contain the inviscid fluxes and the viscous fluxes, respectively.

Following the general procedures for FVM, the governing differential equations may be integrated over an arbitrary volume Λ. Application of the divergence theorem on the convective and viscous flux term integrals yields

$$\begin{aligned} \tfrac{\partial}{\partial t}\textstyle\int_\Lambda \mathbf{w} d\Lambda \quad &+ \textstyle\int_{\partial\Lambda} (\mathbf{f} dS_x + \mathbf{g} dS_y + \mathbf{h} dS_z) \\ &= \textstyle\int_{\partial\Lambda} (\mathbf{f_v} dS_x + \mathbf{g_v} dS_y + \mathbf{h_v} dS_z) \end{aligned} \qquad (5)$$

where S_x, S_y and S_z are the projections of the area $\partial\Lambda$ in the x, y and z directions, respectively. The computational domain is divided into hexahedral cells. Application of FVM to each of the computational cells results in the following system of ordinary differential equations

$$\frac{d}{dt}(\Lambda_{ijk}\mathbf{w}) + C_{ijk} - V_{ijk} = 0$$

where C_{ijk} and V_{ijk} are the discretized evaluations of the convective and viscous flux surface integrals appearing in equation 5 and Λ_{ijk} is the volume of the computational cell. In practice, the discretization scheme reduces to a second order accurate, nondissipative central difference approximation to the bulk flow equations on sufficiently smooth grids. A central difference scheme permits odd-even decoupling at adjacent nodes which may lead to oscillatory solutions. To prevent this "unphysical" phenomena from occurring, a dissipation term is added to the system of equations such that the system now becomes

$$\frac{d}{dt}(\Lambda_{ijk}\mathbf{w}) + [C_{ijk}(\mathbf{w}) - V_{ijk}(\mathbf{w}) - D_{ijk}(\mathbf{w})] = 0. \qquad (6)$$

For the present problem a fourth derivative background dissipation term is added. The dissipative term is constructed in such a manner that the conservation form of the system of equations is preserved. The dissipation term is third order in truncation terms so as not to detract from the second order accuracy of the flux discretization. Equation 6 is integrated in time to steady state using an explicit multistage scheme. For each bulk flow time step, the grid, and thus Λ_{ijk}, is independent of time. Hence equation 6 can be written as

$$\frac{d\mathbf{w}_{ijk}}{dt} + R_{ijk}(\mathbf{w}) = 0 \qquad (7)$$

where the residual is defined as

$$R_{ijk}(\mathbf{w}) = C_{ijk}(\mathbf{w}) - V_{ijk}(\mathbf{w}) - D_{ijk}(\mathbf{w})$$

and the cell volume Λ_{ijk} is absorbed into the residual for clarity.

Full Multigrid Strategy

Rapid convergence to a steady state is achieved with the aid of a multigrid procedure. The idea behind the multigrid strategy is to accelerate evolution of the system of equations on the fine grid by introducing auxiliary calculations on a series of coarse grids. The coarser grid calculations introduce larger scales and larger time steps with the result that low-frequency error components may be efficiently and rapidly damped out.

The multigrid acceleration procedure is embedded in a grid refinement procedure which has the dual purpose of reducing the computer time required to achieve steady state solutions on finely resolved grids, and to allow for a grid convergence study of the computed results. In the grid refinement procedure the flow equations are solved on coarse grids in the early stages of the simulation. The coarse grids permit large time steps, and the flow field and the wave pattern evolve quite rapidly. When the wave pattern reaches a steady state, the grid is refined by doubling the number of grid points in all directions and the flow variables and free surface location are interpolated onto the new grid. Computations then continue using the finer grid. The multigrid procedure is applied at all stages of the grid refinement to accelerate the calculations on each grid in the sequence, producing a composite "full multigrid" scheme which is extremely efficient.

The grid refinement procedure is also extremely important in evaluating the consistency of the computational scheme. As the grid is continually refined a point should be reached whereby further refinement produces no change in the computed results. This method gives an indication of the resolution required to sufficiently capture the details of the particular problem being addressed; if upon further refinement of the grid global

quantities such as drag or lift change, then the resolution is probably insufficient and further refinement may be necessary.

Free Surface Solution

Both a kinematic and dynamic boundary condition must be imposed at the free surface. For the fully nonlinear condition, this requires the free surface to move with the flow (ie. up or down corresponding to the wave height and location) and the boundary conditions to be applied on the distorted free surface. Equation 3 can be cast in a form more amenable to numerical computations by introducing a curvilinear coordinate system that transforms the curved free surface $\beta(x,y)$ into computational coordinates $\beta(\xi,\eta)$. This results in the following transformed kinematic condition

$$\beta_{t^*} + \tilde{u}\beta_\xi + \tilde{v}\beta_\eta = w \tag{8}$$

where $\tilde{u}$ and $\tilde{v}$ are contravariant velocity components given by

$$\tilde{u} = u\xi_x + v\xi_y = (uy_\eta - vx_\eta)J^{-1}$$

$$\tilde{v} = u\eta_x + v\eta_y = (vx_\xi - uy_\xi)J^{-1}$$

and $J = x_\xi y_\eta - x_\eta y_\xi$ is the Jacobian.

Equation 8 is essentially a linear hyperbolic equation, which in our original method was discretized by central differences augmented by high order diffusion [8, 9]. Such a scheme can be obtained by introducing anti-diffusive terms in a standard first order formula. In particular, it is well known that for a one-dimensional scalar equation model, central difference approximation of the derivative may be corrected by adding a third order dissipative flux:

$$d_{j+\frac{1}{2}} = \alpha_{j+\frac{1}{2}} \left\{ \Delta\beta_{j+\frac{1}{2}} - \frac{1}{2}\left(\Delta\beta_{j+\frac{3}{2}} + \Delta\beta_{j-\frac{1}{2}}\right)\right\} \tag{9}$$

where $\alpha_{j+\frac{1}{2}} = |\tilde{u}_{j+\frac{1}{2}}|$ at the cell interface. This is equivalent to the scheme which we have used until now to discretize the free surface, and which has proven to be effective for simple hulls. However, on more complex configuration of interest, such as combatant vessels and yachts, the physical wave at the bow tends to break. This phenomenon cannot be fully accounted for in the present mathematical model. In order to avoid the overturning of the wave and continue the calculations lower order dissipation must be locally introduced in a controlled manner. This can be accomplished by borrowing from the theory of non-oscillatory schemes constructed using the Local Extremum Diminishing (LED) principle [13]. These include Symmetric Limited Positive (SLIP) and UpStream Limited Positive (USLIP) schemes. A brief description of these methods is presented next.

Symmetric LImited Positive (SLIP) scheme

Let $L(p,q)$ be a limited average of p and q with the following properties:

P1. $L(p,q) = L(q,p)$

P2. $L(\alpha p, \alpha q) = \alpha L(p,q)$

P3. $L(p,p) = p$

P4. $L(p,q) = 0$ if p and q have opposite signs.

The diffusive flux for a scalar conservation law is now defined as

$$d_{j+\frac{1}{2}} = \alpha_{j+\frac{1}{2}} \left\{ \Delta\beta_{j+\frac{1}{2}} - L\left(\Delta\beta_{j+\frac{3}{2}}, \Delta\beta_{j-\frac{1}{2}}\right)\right\}. \tag{10}$$

This construction will be referred to as the Symmetric LImited Positive (SLIP) scheme.

The requirement P4 on $L(p,q)$ is the key for constructing an LED scheme. If $\Delta\beta_{j+\frac{3}{2}}$ and $\Delta\beta_{j-\frac{1}{2}}$ have opposite signs then there is an extremum at either j or $j+1$. In the case of an odd-even mode, however, they have the same sign, which is opposite to that of $\Delta\beta_{j+\frac{1}{2}}$, so that they reinforce the damping in the same way that a simple central fourth difference formula would.

UpStream LImited Positive (USLIP) scheme

By adding the anti-diffusive correction purely from the upstream side one may derive a family of UpStream LImited Positive (USLIP) schemes. Corresponding to the original SLIP scheme defined by equation (10), a USLIP scheme is obtained by setting

$$\begin{aligned} d_{j+\frac{1}{2}} &= \alpha_{j+\frac{1}{2}} \left\{ \Delta\beta_{j+\frac{1}{2}} - L\left(\Delta\beta_{j+\frac{1}{2}}, \Delta\beta_{j-\frac{1}{2}}\right)\right\} \\ &\text{if} \quad \tilde{u}_{j+\frac{1}{2}} > 0 \\ d_{j+\frac{1}{2}} &= \alpha_{j+\frac{1}{2}} \left\{ \Delta\beta_{j+\frac{1}{2}} - L\left(\Delta\beta_{j+\frac{1}{2}}, \Delta\beta_{j+\frac{3}{2}}\right)\right\} \\ &\text{if} \quad \tilde{u}_{j+\frac{1}{2}} < 0 \end{aligned}$$

The breaking of a wave is generally characterized by a change in sign of the velocity across the crest. Thus limiting the antidiffusion purely from the upstream side may be more suitable to stabilize the calculations and avoid the overturning of the waves.

Flux Limiters

A variety of limiters may be defined which meet the requirements (P1 –P4). In particular, by defining

$$S(p,q) = \frac{1}{2}\{\text{sign}(p) + \text{sign}(q)\}$$

so that

$$S(p,q) = \begin{cases} 1 & \text{if } p > 0 \text{ and } q > 0 \\ 0 & \text{if } p \text{ and } q \text{ haqe opposite sign} \\ -1 & \text{if } p < 0 \text{ and } q < 0 \end{cases}$$

one may easily implement any of the three well known limiters: minmod, Van Leer, or superbee, or construct alternative limiters starting from the more general formulas presented in reference [13]. In the present study

Properties P1–P3 are natural properties of an average, whereas P4 is needed for the construction of an LED scheme.

we use a simple limiter (α-mean) which limits the arithmetic mean by some multiple of the smaller of $|p|$ or $|q|$. It may be cast in the following form:

$$L(p,q) = S(p,q)\min\left(\frac{|p+q|}{2},\ \alpha|p|,\ \alpha|q|\right).$$

It is well known that schemes which strictly satisfy the LED principle fall back to first order accuracy at extrema even when they realize higher order accuracy elsewhere. This difficulty can be circumvented by relaxing the LED requirement. Therefore the concept of essentially local extremum diminishing (ELED) schemes is introduced as an alternative approach. These are schemes for which, in the limit as the mesh width $\Delta x \to 0$, maxima are non-increasing and minima are non-decreasing.

In order to prevent the limiter from being active at smooth extrema it is convenient to set

$$L(p,q) = \frac{1}{2}D(p,q)(p+q)$$

where $D(p,q)$ is a factor which should deflate the arithmetic average, and become zero if u and v have opposite signs. Take

$$D(p,q) = 1 - R(p,q) \tag{11}$$

where

$$R(p,q) = \left|\frac{p-q}{\max(|p|+|q|,\epsilon\Delta x^r)}\right|^s \tag{12}$$

and $\epsilon > 0$, r is a positive power, and s is a positive integer. Then $D(p,q) = 0$ if p and q have opposite signs. Also if $s = 1$, $L(p,q)$ reduces to minmod, while if $s = 2$, $L(p,q)$ is equivalent to Van Leer's limiter. By increasing s one can generate a sequence of limited averages which approach a limit defined by the arithmetic mean truncated to zero when p and q have opposite signs. These smooth limiters are known to have a benign effect on the convergence to a steady state of compressible flows.

Discretization, Integration and Comments

The free surface kinematic equation may be expressed as

$$\frac{d\beta_{ij}}{dt^*} + Q_{ij}(\beta) = 0$$

where $Q_{ij}(\beta)$ consists of the collection of velocity and spatial gradient terms which result from the discretization of equation 8.

The spatial discretization of 8 is carried out as follows. Throughout the interior of the distorted free surface all derivatives for $\beta(\xi,\eta)$ are computed using the second order centered difference stencil in computational coordinates ξ and η. On the boundaries a second order centered stencil is used along the boundary tangent and a first order one sided difference stencil is used in the boundary normal direction. The contravariant velocity components are computed at each centroid of the four surface cell faces surrounding node ij and averaged at the node. The velocity component w is the present nodal value. Different methods of accomplishing the spatial discretization are readily available, but this method has proved to be robust and has thus been adopted.

The same scheme used to integrate equation 7 is also used here.

Once the free surface update is accomplished the pressure is adjusted on the free surface such that

$$\psi^{(n+1)} = \beta^{(n+1)}Fr^{-2}.$$

The free surface and the bulk flow solutions are coupled by first computing the bulk flow at each time step, and then using the bulk flow velocities to calculate the movement of the free surface. After the free surface is updated, its new values are used as a boundary condition for the pressure on the bulk flow for the next time step. The entire iterative process, in which both the bulk flow and the free surface are updated at each time step, is repeated until some measure of convergence is attained: usually steady state wave profile and wave resistance coefficient.

Since the free surface is a material surface, the flow must be tangent to it in the final steady state. During the iterations, however, the flow is allowed to *leak* through the surface as the solution evolves towards the steady state. This leakage, in effect, drives the evolution equation. Suppose that at some stage, the vertical velocity component w is positive (cf. equation 3 or 8). Provided that the other terms are small, this will force β^{n+1} to be greater than β^n. When the time step is complete, ψ is adjusted such that $\psi^{n+1} > \psi^n$. Since the free surface has moved farther away from the original undisturbed upstream elevation and the pressure correspondingly increased, the velocity component w (or better still $\mathbf{q}\cdot\mathbf{n}$ where $\mathbf{n} = \frac{\nabla F}{|\nabla F|}$ and $F = z - \beta(x,y)$) will then be reduced. This results in a smaller $\Delta\beta$ for the next time step. The same is true for negative vertical velocity, in which case there is mass leakage into the system rather than out. Only when steady state has been reached is the mass flux through the surface zero and tangency enforced. In fact, the residual flux leakage could be used in addition to drag components and pressure residuals as a measure of convergence to the steady state.

This method of updating the free surface works well for the Euler equations since tangency along the hull can be easily enforced. However, for the Navier-Stokes equations the no-slip boundary condition is inconsistent with the free surface boundary condition at the hull/waterline intersection. To circumvent this difficulty the computed elevation for the second row of grid points away from the hull is extrapolated to the hull. Since the minimum spacing normal to the hull is small, the error due to this should be correspondingly small, comparable with other discretization errors. The treatment of this intersection for the Navier-Stokes calculations, should be the subject of future research to find the most accurate possible procedure.

Results

This section includes results using the baseline USLIP-LED scheme with the $\alpha-$mean limiter. The first set of

results for a Series 60 ship hull provides a validation of the scheme for both Euler and RANS model by comparison with available experimental data.

A naval frigate with sonar dome and transom stern is utilized to compare three different free-surface discretization schemes. This typical configuration of a combatant ship provides a severe test case for our schemes since it is known that both the bow and the stern waves tend to break.

The last set of calculations on an IACC sailing yacht with rudder, keel and ballast bulb demonstrate the capability of our method to deal with complex configurations.

Series 60, Cb = 0.6 Hull

Results for both viscous and inviscid simulations about the Series 60 hull are presented. Figures 2 - 6 are used to display the results of the simulations.

Figure 2 shows the computed intersection between the waterline and hull vs. the experimental data. In both viscous and inviscid flow cases, excellent agreement is obtained, from bow to stern, between computation and experiment. Figure 3 shows the wave drag C_w history for the inviscid calculations, and the residuary drag C_r, frictional drag C_f and total drag histories C_t for the viscous calculations. The computed drag histories show good grid convergence toward unique, grid independent solutions as the grid is refined, every 500 multigrid cycles, by doubling the number of grid points in each coordinate direction. Note that the drag quantities reach near final values well before 500 multigrid cycles on the fine grid; the large number of cycles is required only to obtain well developed overhead wave patterns. The final numerical values of drag are in excellent agreement with those determined experimentally [1, 2]. Figure 4 shows an overhead view of the computed wave elevations for both the viscous and inviscid simulations. It is interesting to note that, with the exception of the stern region, the flow field exhibits essentially an inviscid behavior. Finally, figures 5 and 6 show a detailed comparison of the computed u, v and w velocity components, pressure p and total head H vs. experimental data obtained by traversing the viscous boundary layer at stations $x = 0.4$ and 0.8 downstream of the bow, and at three elevations $z = -0.01$, -0.03 and -0.05 along the draft. The agreement with experiment at these locations, where the boundary layer is fully developed and attached, is excellent.

Combatant Ship with Transom Stern

Results are presented for calculations using a naval frigate as the model geometry. Several complications arise on this particular hull due to the presence of a transom stern. The presence of the transom requires some modifications to the free surface routine used for general displacement type hulls - ie. hulls with no discontinuity in the slope of the hull below the free surface. The plane of the transom stern makes essentially a right angle with the bottom of the hull and care must be taken in constructing the initial grid such that the trailing edge row of grid points on the free surface are tangent to the stern. Also, a Kutta-like condition is imposed at the transom by enforcing a flow which exits the stern tangentially at the intersection with the bottom of the hull (fixed elevation). All the results presented are for a Froude number of 0.2067. A comparison of the waterline computed by a USLIP-LED with $\alpha-$mean limiters, a SLIP scheme with $\alpha-$mean limiter, and a USLIP-ELED formulation are shown in figure 7a. It can be seen that the results computed by the three schemes compare reasonably well with each other as well as with the experimental data. The only notable exception is at the crest of the bow wave where the $\alpha-$mean limited schemes exhibit a lower peak consistent with the larger amount of dissipation which is introduced near extrema. The peak computed by the USLIP-ELED is in very good agreement with experiments. A similar trend is exhibited by the results obtained for the RANS simulations which are also presented in 7b. The USLIP-ELED approach also gives a slightly better resolution of the divergent wave for both the Euler and RANS models. This is shown in figures 7c - 7d where the contours of the wave elevation computed by the USLIP-LED and USLIP-ELED approach are presented.

A convergence study of the drag computed by the three schemes is summarized in table 1. One can observe that the final drag coefficients computed by the three schemes agree to within 5%.

IACC Yacht Hull

The versatility of the method is further illustrated using the computed results for the flow about an International America's Cup Class (IACC) type yacht hull. Hulls of this type present challenging modeling difficulties in that the presence of appendages must be taken into account, as well as the large degree of "stern overhang." The inclusion of appendages is essentially a grid generation issue and does not present major difficulties to the flow solver. The stern overhang, which forces the grid to move aft as the stern wake is being formed, may also be accommodated through extreme care in the initial grid generation.

Figure 8 shows an overhead view of the computed wave patterns for a bare hull translating at 11 knots. Note the similarity between both inviscid and viscous cases except near the stern where separation is present. This is also evident by comparing the computed waterlines in figure 9. These figures also provide a clear indication of the effect produced by the stern overhang.

Figure 10 and 11 show the large degree of grid distortion that the free surface routines permit. In this case the steep gradient of the free surface elevation indicates that wave breaking conditions may develop. Although physically correct, this situation would lead to immediate numerical instability. Effective treatment of fully three dimensional breaking waves is an area of research where little progress has been made. In our approach, the steep gradient is cleanly captured by the action of

the limiter which turns off, locally, the antidiffusion. This technique holds the steep wave in place, and allows the continuation of the calculation.

The remaining figures, 12 - 13, show the results for a recent Euler calculation about a full configuration IACC yacht. The yacht is translating in an upright position at 9 knots and a 5 degree angle-of-attack. Since this is an angle-of-attack calculation, a second grid block was required and the symmetry plane boundary conditions were removed at the joining block interfaces. Approximately 2.75 million grid points were used in the calculation.

Discussion and Future Work

Two USLIP schemes, one based on the local extremum diminishing principle and the other on the essential local extremum diminishing principle, have been incorporated into the basic ship wave solver presented in references [8, 9]. A grid convergence study on a combatant ship with a transom stern indicated that the USLIP-ELED formulation yields slightly more accurate results especially near extrema. However, we found that the USLIP-LED formulation may be more robust in dealing with very steep waves and it has allowed the simulation of the free surface flow about configurations representative of realistic hull geometries including a complete configuration of a IACC yacht.

With the exception of the complete configuration IACC yacht, all the calculations were run on an IBM RISC workstations and the calculations were performed using between 2.5 and 10 hours of CPU time. The grids for these calculations used approximately 1 million points each. The fully configured IACC yacht required a grid with nearly 2.75 million points. This calculation took approximately 30 hours on a Convex C220 computer using approximately 750 Mbytes of main memory.

A parallel implementation of the computer code is currently underway. Preliminary timing with similar flow codes indicates that computational times of the order of one half hour per viscous simulation are attainable. This will provide the fast turn-around which is required for the effective and routine use of non-linear RANS simulation within the design process.

Acknowledgment

Our work has benefited greatly from the support of the Office of Naval Research through Grant N00014-93-I-0079, under the supervision of Dr. E.P. Rood.

References

[1] Toda,Y., Stern,F., and Longo,J., "Mean-Flow Measurements in the Boundary Layer and Wake and Wave Field of a Series 60 $C_B = 0.6$ Ship Model–Part1: Froude Numbers 0.16 and 0.316," *Journal of Ship Research,* v. 36, n. 4, pp. 360-377, 1992.

[2] Longo,J., Stern,F., and Toda,Y., "Mean-Flow Measurements in the Boundary Layer and Wake and Wave Field of a Series 60 $C_B = 0.6$ Ship Model–Part2: Effects on Near-Field Wave Patterns and Comparisons with Inviscid Theory," *Journal of Ship Research,* v. 37, n. 1, pp. 16-24, 1993.

[3] Hino,T., "Computation of Free Surface Flow Around an Advancing Ship by the Navier-Stokes Equations," *Proceedings, Fifth International Conference on Numerical Ship Hydrodynamics,* pp. 103-117, 1989.

[4] Miyata,H., Zhu,M., and Wantanabe,O., "Numerical Study on a Viscous Flow with Free-Surface Waves About a Ship in Steady Straight Course by a Finite-Volume Method," *Journal of Ship Research,* v. 36, n. 4, pp. 332-345, 1992.

[5] Tahara,Y., Stern,F., and Rosen,B., "An Interactive Approach for Calculating Ship Boundary Layers and Wakes for Nonzero Froude Number," *Journal of Computational Physics,* v. 98, pp. 33-53, 1992.

[6] Chen,H.C., Patel,V.C., and Ju,S., "Solution of Reynolds-Averaged Navier-Stokes Equations for Three-Dimensional Incompressible Flows," *Journal of Computational Physics,* v. 88, pp. 305-336, 1990.

[7] Rosen,B.S., Laiosa,J.P., Davis,W.H., and Stavetski,D., "SPLASH Free-Surface Flow Code Methodology for Hydrodynamic Design and Analysis of IACC Yachts,", *The Eleventh Chesapeake Sailing Yacht Symposium,* Annapolis, MD, 1993.

[8] Farmer,J.R., Martinelli,L., and Jameson,A., "A Fast Multigrid Method for Solving Incompressible Hydrodynamic Problems with Free Surfaces," *AIAA Journal,* v. 32, no. 6, pp. 1175-1182, 1994.

[9] Farmer,J.R., Martinelli,L., and Jameson,A., "A Fast Multigrid Method for Solving the Nonlinear Ship Wave Problem with a Free Surface," *Proceedings, Sixth International Conference on Numerical Ship Hydrodynamics,* pp. 155-172, 1993.

[10] Jameson,A., "A Vertex Based Multigrid Algorithm For Three Dimensional Compressible Flow Calculations," *ASME Symposium on Numerical Methods for Compressible Flows,* Annaheim, December 1986.

[11] Baldwin,B.S., and Lomax,H., "Thin Layer Approximation and Algebraic Model for Separated Turbulent Flows," *AIAA Paper 78-257, AIAA 16th Aerospace Sciences Meeting,* Reno, NV, January 1978.

[12] Chorin,A., "A Numerical Method for Solving Incompressible Viscous Flow Problems," *Journal of Computational Physics,* v. 2, pp. 12-26, 1967.

[13] Jameson,A., "Computational Algorithms for Aerodynamic Analysis and Design," MAE Report 1966, Princeton University, December, 1992.

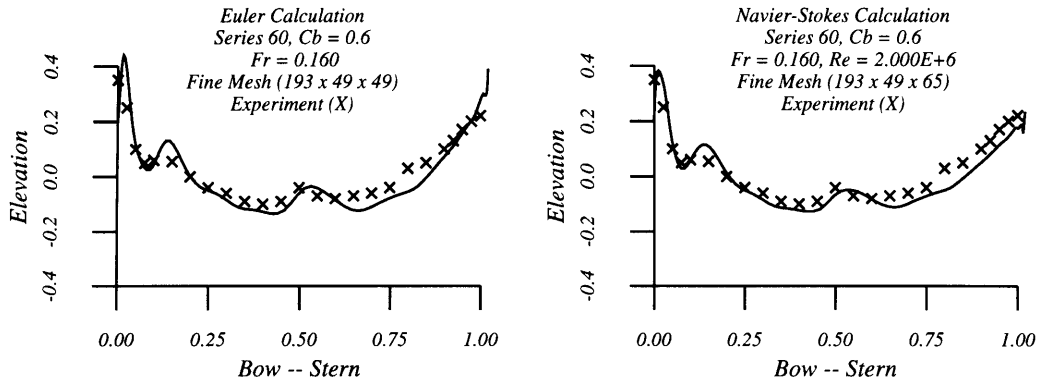

Figure 2: Computed Hull Wave Profiles vs. Experiment.

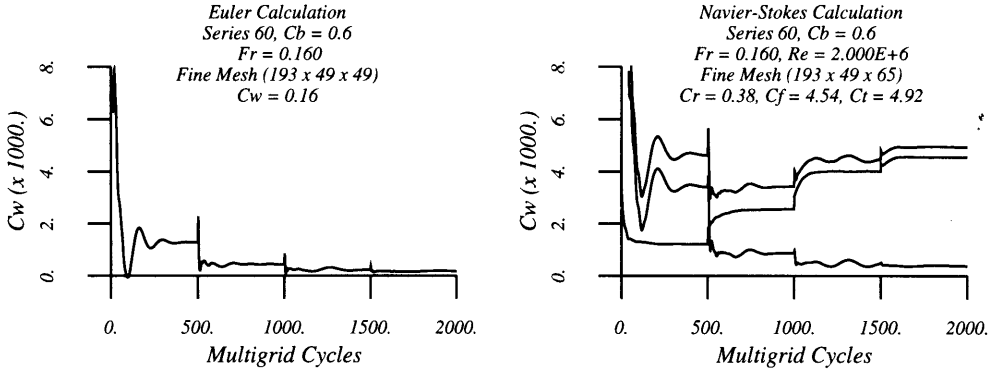

Figure 3: Computed Drag History.

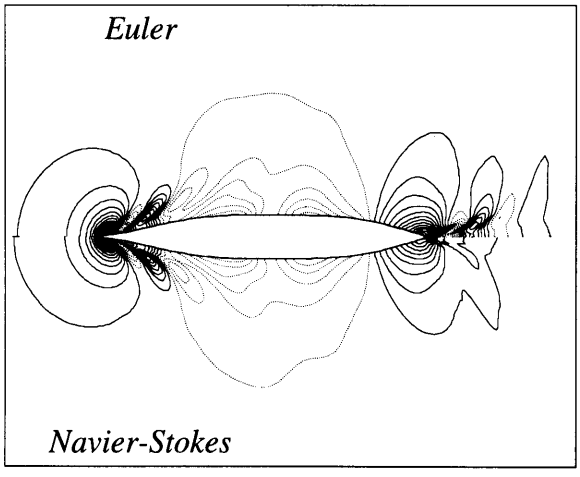

Figure 4: Comparison of Computed Overhead Wave Contours, Fr = 0.160.

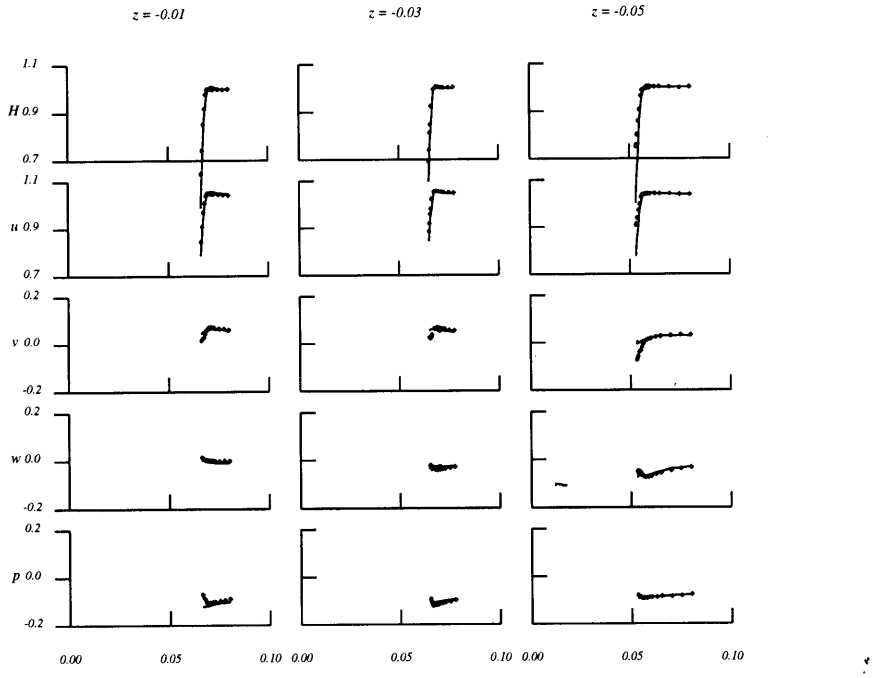

Figure 5: Total Head, Velocity and Pressure Profiles, x = 0.4, Fr = 0.160, Re = $2x10^6$.

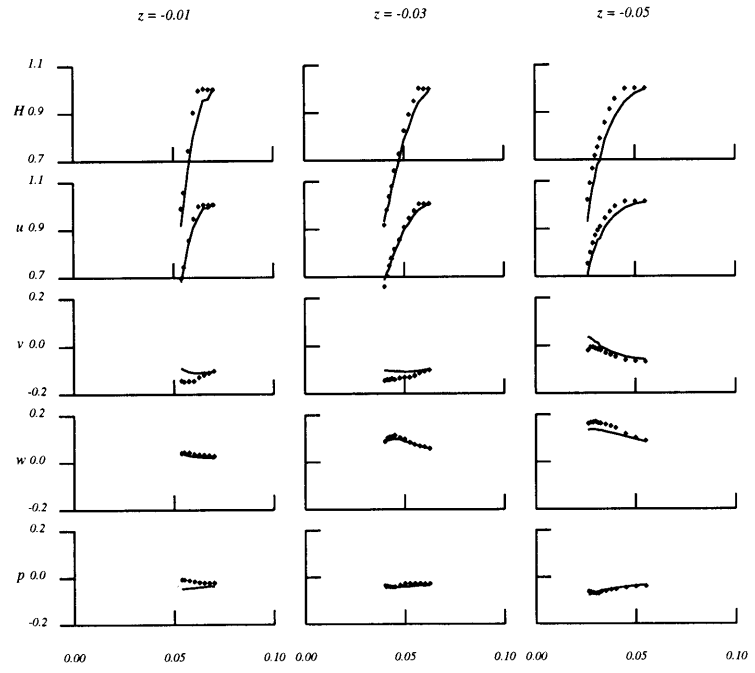

Figure 6: Total head, Velocity and Pressure Profiles, x = 0.8, Fr = 0.160, Re = $2x10^6$.

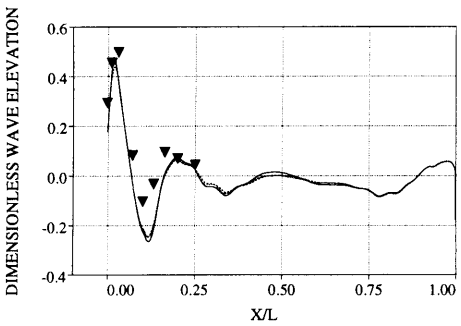

7a: Computed – Measured Waterlines
Euler Equations – $289 \times 49 \times 65$.

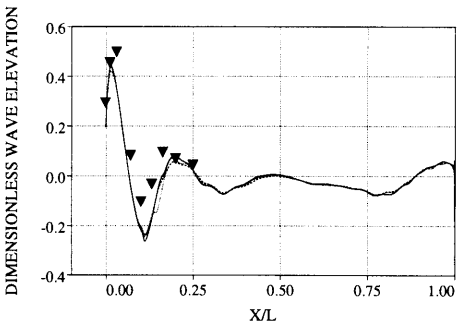

7b: Computed – Measured Waterlines
RANS Equations – $289 \times 49 \times 65$.

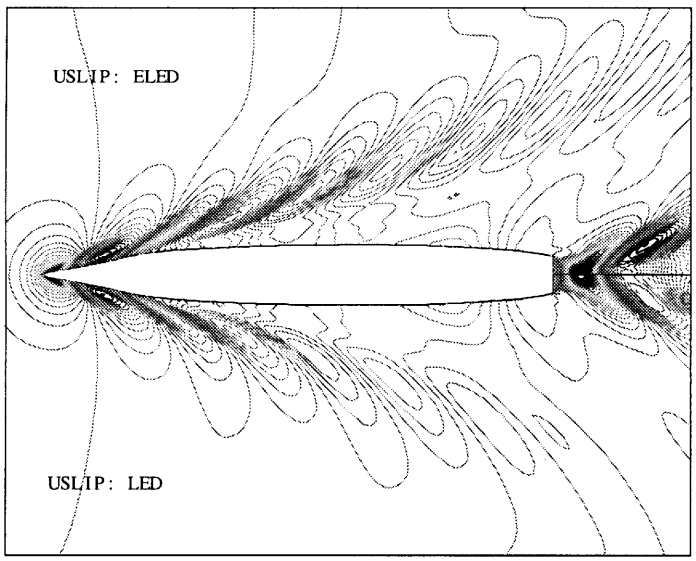

7c: Computed wave elevation – Euler Equations
$289 \times 49 \times 65$.

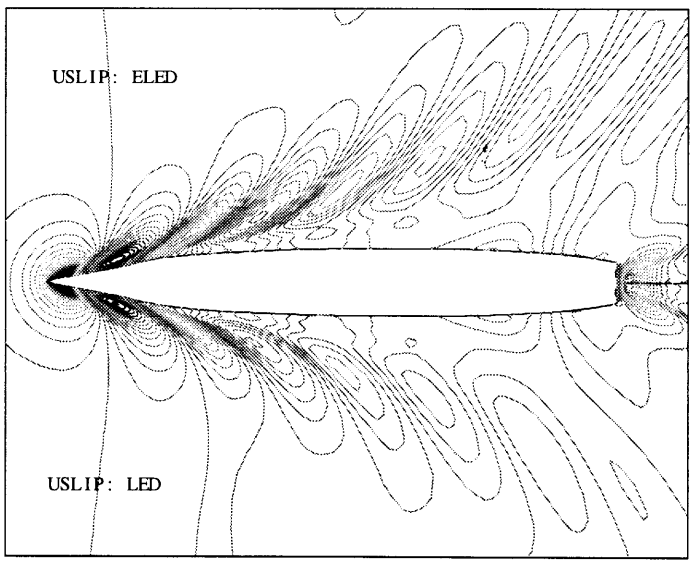

7d: Computed wave elevation – RANS Equations –
$289 \times 49 \times 65$.

Figure 7: Comparison of computed wave elevations using the Euler (left) and RANS (right) equations.

	USLIP			SLIP			ELED		
Resolution	C_t	C_f	C_r	C_t	C_f	C_r	C_t	C_f	C_r
$73 \times 13 \times 17$	5.13	2.04	3.09	5.12	2.08	3.04	4.98	2.04	2.97
$145 \times 25 \times 33$	5.01	3.39	1.62	5.10	3.50	1.60	5.07	3.39	1.68
$289 \times 49 \times 65$	5.15	4.06	1.09	5.24	4.06	1.18	5.24	4.04	1.20

Table 1: Grid convergence study of the computed drag coefficients ($\times 1000.$).

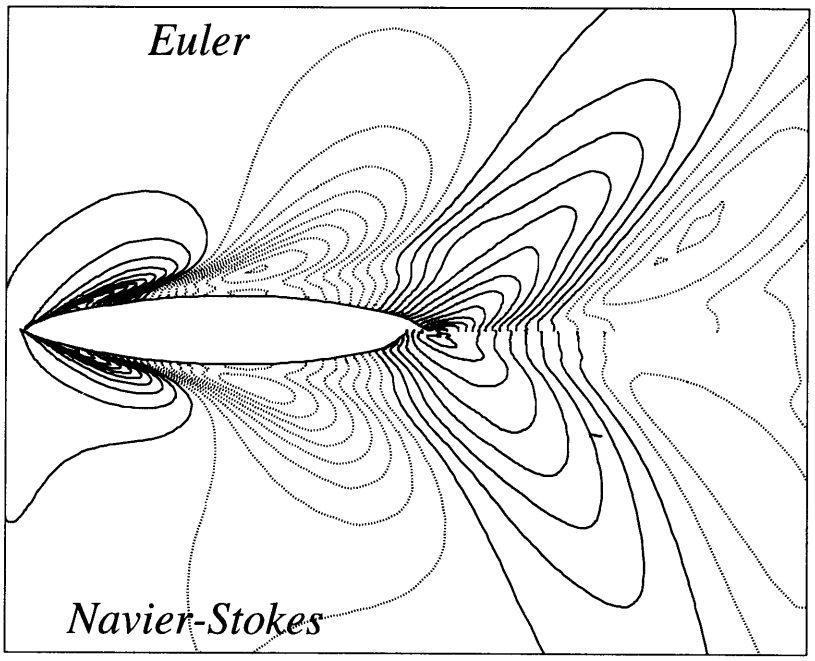

Figure 8: Comparison of Computed Overhead Wave Profiles, 11 knots.

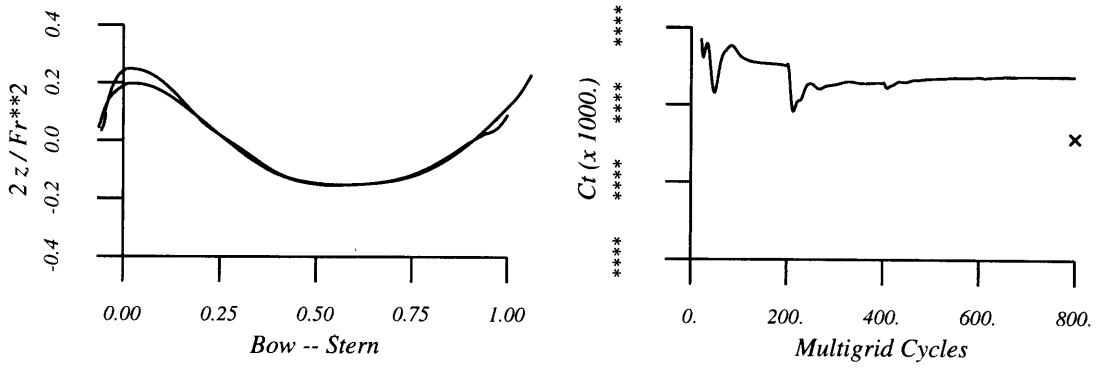

Figure 9: Bare Hull Wave Profiles and Drag History.

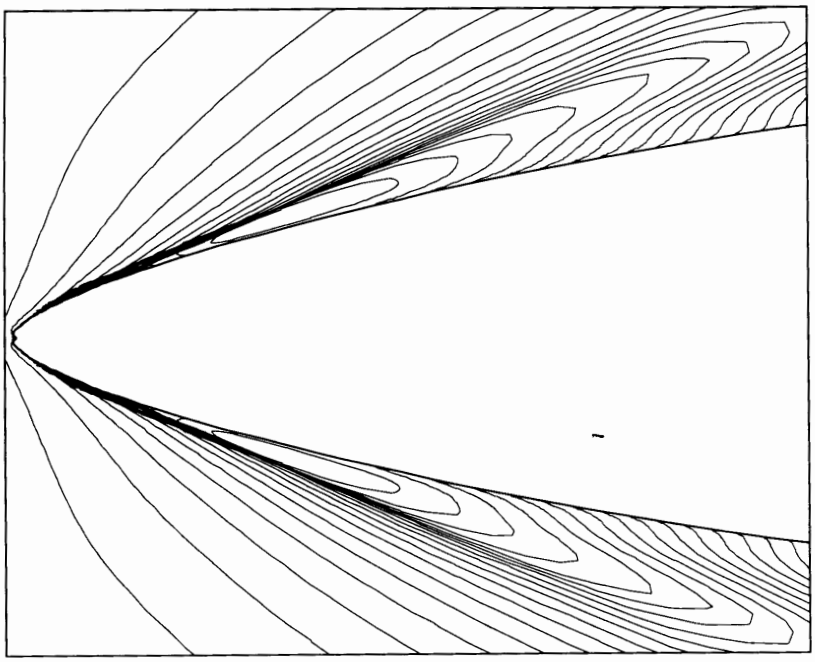

Figure 10: Overhead View of Bow Wave Contours.

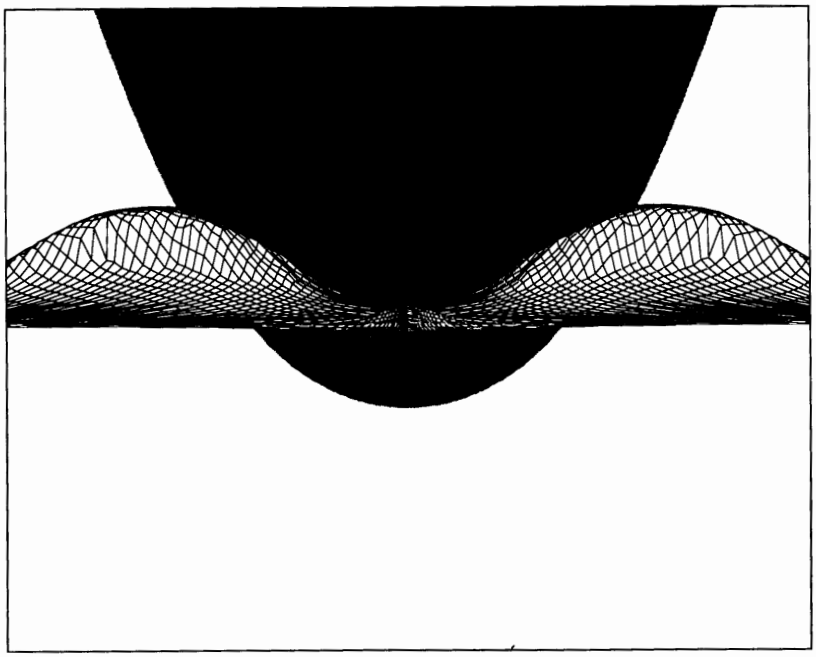

Figure 11: Frontal View of Bow Wave Distorted Grid.

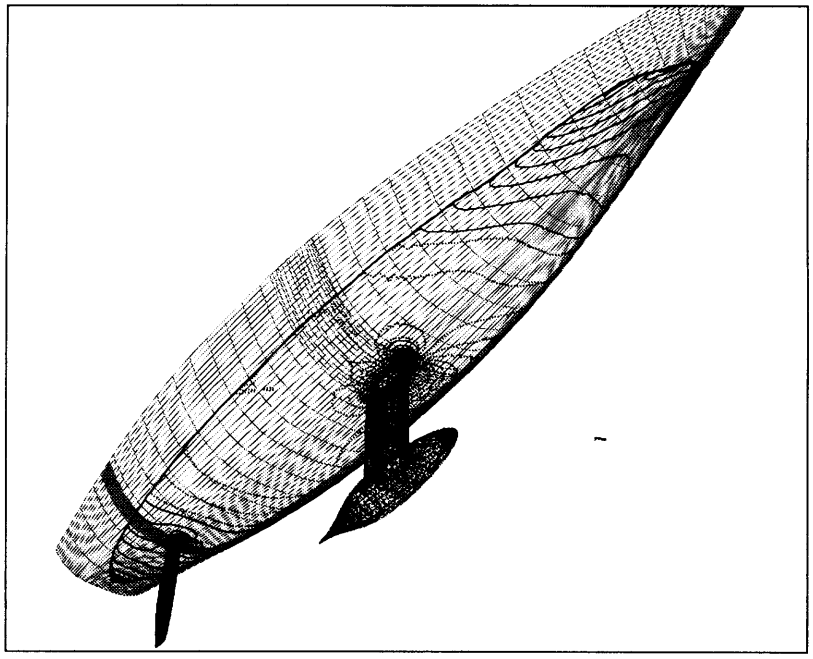

Figure 12: Pressure Contours on Hull and Appendages.

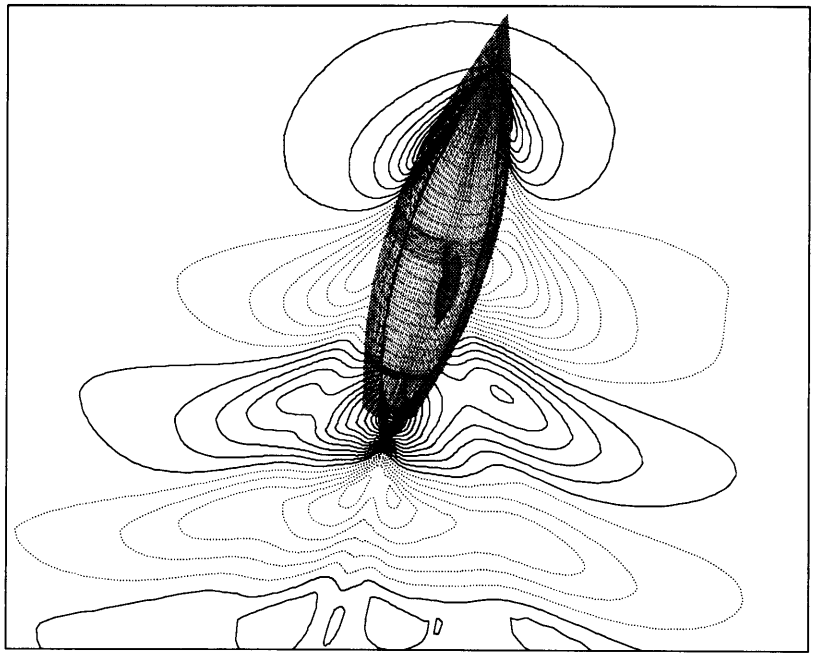

Figure 13: Pressure Contours on Free Surface.